Broad parameter optimization of polarization-diversity 2D grating couplers for silicon photonics

Lee Carroll,[1] Dario Gerace,[1] Ilaria Cristiani,[2] Sylvie Menezo,[3] and Lucio C. Andreani[1]

[1]*Department of Physics, University of Pavia, Via Bassi 6, I-27100 Pavia, Italy*
[2]*Department of Electrical, Computer and Biomedical Engineering, University of Pavia, Via Ferrata 1, I-27100 Pavia, Italy*
[3]*CEA-LETI-MINATEC, 17 Rue des Martyrs, 38050 Grenoble Cedex 9, France*
[*]*lee.carroll@unipv.it*

Abstract: Polarization-diversity couplers, which are designed to couple the unknown polarization state of an optical fiber into the TE-polarized modes of integrated waveguides, are important for the development of practical all-optical circuits. We describe the use of a full 3D finite difference time domain (FDTD) calculation campaign to rigorously optimize the 2D photonic crystal grating that couples a single-mode telecom fiber to the silicon waveguides of a Silicon-on-Insulator (SOI) platform. With this approach we identify the unique optimum combination of etch-depth, hole-radius, and grating-pitch of the photonic crystal array for best performance at 1550 nm. The mean (polarization-averaged) coupling efficiency of 48% (−3.2dB) exceeds reported efficiencies of analogous couplers, and has only a marginal dependence on the polarization state of the input fiber (48 ± 3%). In addition, 3D-FDTD calculations are used to characterize the propagation direction, mode-profile, and polarization of light coupled from the fiber into the SOI slab. Such information is crucial for component design and goes beyond previously available results from existing approximations and simulations of 2D-grating coupler performance. Calculations of photonic mode dispersion in the grating coupler, by means of guided-mode expansion, indicate that the coupling is due to an optically active resonant guided mode in the photonic crystal array. This points towards a fast optimization scheme that enhances both the performance and the physical interpretation of 3D-FDTD simulations.

OCIS codes: (050.1755) Computational electromagnetic methods; (050.5298) Photonic crystals; (130.1750) Components; (130.5440) Polarization-selective devices.

References and links

1. G. Roelkens, D. Van Thourhout, and R. Baets, "High efficiency grating coupler between silicon-on-insulator waveguides and perfectly vertical optical fibers," Opt. Lett. **32**(11), 1495–1497 (2007).
2. F. Van Laere, M. V. Kotlyar, D. Taillaert, D. Van Thourhout, T. F. Krauss, and R. Baets, "Compact slanted grating couplers between optical fiber and InP–InGaAsP waveguides," IEEE Photon. Technol. Lett. **19**(6), 396–398 (2007).
3. D. Taillaert, P. Bienstman, and R. Baets, "Compact efficient broadband grating coupler for silicon-on-insulator waveguides," Opt. Lett. **29**(23), 2749–2751 (2004).
4. D. Taillaert, F. Van Laere, M. Ayre, W. Bogaerts, D. Van Thourhout, P. Bienstman, and R. Baets, "Grating couplers for coupling between optical fibers and nanophotonic waveguides," Jpn. J. Appl. Phys. **45**(8A), 6071–6077 (2006).
5. D. Taillaert, W. Bogaerts, P. Bienstman, T. F. Krauss, P. Van Daele, I. Moerman, S. Verstuyft, K. De Mesel, and R. Baets, "An out-of-plane grating coupler for efficient butt-coupling between compact planar waveguides and single-mode fibers," IEEE J. Quantum Electron. **38**(7), 949–955 (2002).
6. M. Antelius, K. B. Gylfason, and H. Sohlström, "An apodized SOI waveguide-to-fiber surface grating coupler for single lithography silicon photonics," Opt. Express **19**(4), 3592–3598 (2011).

7. G. Roelkens, D. Vermeulen, D. Van Thourhout, R. Baets, S. Brision, P. Lyan, P. Gautier, and J.-M. Fédéli, "High efficiency diffractive grating couplers for interfacing a single mode optical fiber with a nanophotonic silicon-on-insulator waveguide circuit," Appl. Phys. Lett. **92**(13), 131101 (2008).
8. L. Liu, M. Pu, K. Yvind, and J. M. Hvam, "High-efficiency, large-bandwidth silicon-on-insulator grating coupler based on a fully-etched photonic crystal structure," Appl. Phys. Lett. **96**(5), 051126 (2010).
9. X. Chen and H. K. Tsang, "Polarization-independent grating couplers for silicon-on-insulator nanophotonic waveguides," Opt. Lett. **36**(6), 796–798 (2011).
10. T. Yongbo, D. Daoxin, and H. Sailing, "Proposal for a grating waveguide serving as both a polarization splitter and an efficient coupler for silicon-on-insulator nanophotonic circuits," IEEE Photon. Technol. Lett. **21**(4), 242–244 (2009).
11. D. Taillaert, H. Chong, P. I. Borel, L. H. Frandsen, R. M. De La Rue, and R. Baets, "A compact two-dimensional grating coupler used as a polarization splitter," IEEE Photon. Technol. Lett. **15**(9), 1249–1251 (2003).
12. F. Van Laere, T. Stomeo, D. Taillaert, G. Roelkens, D. Van Thourhout, T. F. Krauss, and R. Baets, "Efficient polarization diversity grating couplers in bonded InP-membrane," IEEE Photon. Technol. Lett. **20**(4), 318–320 (2008).
13. F. Van Laere, T. Stomeo, C. Cambournac, M. Ayre, R. Brenot, H. Benisty, G. Roelkens, T. F. Krauss, D. Van Thourhout, and R. Baets, "Nanophotonic Polarization Diversity Demultiplexer Chip," J. Lightwave Technol. **27**(4), 417–425 (2009).
14. W. Bogaerts, D. Taillaert, P. Dumon, D. Van Thourhout, R. Baets, and E. Pluk, "A polarization-diversity wavelength duplexer circuit in silicon-on-insulator photonic wires," Opt. Express **15**(4), 1567–1578 (2007).
15. F. Van Laere, W. Bogaerts, P. Dumon, G. Roelkens, D. Van Thourhout, and R. Baets, "Focusing polarization diversity grating couplers in silicon-on-insulator," J. Lightwave Technol. **27**(5), 612–618 (2009).
16. S. Pathak, M. Vanslembrouck, P. Dumon, D. Van Thourhout, and W. Bogaerts, "Compact SOI-based polarization diversity wavelength de-multiplexer circuit using two symmetric AWGs," Opt. Express **20**(26), B493–B500 (2012).
17. L. C. Andreani and D. Gerace, "Photonic crystal slabs with a triangular lattice of triangular holes investigated using a guided mode expansion method," Phys. Rev. B **73**(23), 235114 (2006).
18. M. Galli, D. Bajoni, M. Belotti, F. Paleari, M. Patrini, G. Guizzetti, D. Gerace, M. Agio, L. C. Andreani, D. Peyrade, and Y. Chen, "Measurement of Photonic Mode Dispersion and Linewidths in Silicon-on-Insulator Photonic Crystal Slabs," IEEE J. Sel. Areas Comm. **23**(7), 1402–1410 (2005).

1. Introduction

In the last decade there has been a considerable push towards developing integrated silicon photonic circuits to support low-cost information and communication technology applications (ICT). Si-photonic systems combine low cost complementary metal oxide semiconductor (CMOS) fabrication technology from microelectronics with the high optical transmission and refractive index contrast of the SOI (silicon–on-insulator) platform that enables small device footprints with strong optical confinement. The practical realization of Si photonic circuits compatible with the mass-production needed for optical communications systems still faces a number of challenges, and a significant research effort is currently focused on the optimization and integration of components and devices. One on-going challenge is identifying the best low-cost scalable approach for coupling light from a telecom fibre into a Si-photonic circuit with high efficiency. The problem here is two-fold – (i) the single-mode mean-field diameter (MFD) of a fibre is ≈10μm, while the SOI waveguide cross-section is ≈500nm × 220nm, and (ii) the polarization-state of the fibre is generally unknown and unstable, while many Si-photonic circuits contain elements optimized for TE-polarized light only.

One CMOS-compatible solution to bridging the dimensional gap between fibre mode and SOI layer thickness is a grating-coupler that is lithographically-etched into the SOI layer. With a relatively high alignment tolerance that supports low-cost mass production, such grating couplers have a footprint comparable to the fibre mode and diffract light with high efficiency into collection tapers etched into the SOI slab. While some novel designs have been put forward that operate with normal-incidence butt-coupling [1,2], the fibre mode is usually incident on the grating coupler with a small angle-of-incidence (≈10°), to improve the directionality of the diffraction and to reduce back-reflections into the fibre. With the most sophisticated designs, a non-uniform apodized 1D-grating coupler with a distributed Bragg reflector can theoretically have a coupling efficiency of 92% (−0.35dB) [3–5]. Experimental measurements of different 1D-grating coupler designs have given measured coupling efficiencies up to 70% [6–8], showing that high efficiency coupling with grating couplers can be practically realized. However, while 1D-grating couplers are a low-cost CMOS-compatible solution that offer high coupling efficiency, they generally exhibit a very strong sensitivity to the input polarisation state of the fibre, which makes them unsuitable for many inter-system coupling applications.

Although some novel designs based on sub-wavelength patterning of 1D-grating couplers with electron-beam lithography have been proposed as a mean of overcoming the polarization issue [9,10], a more direct solution is the notional superimposition of two orthogonally orientated 1D-grating couplers to form a two dimensional (2D) grating coupler [11]. With this scheme, all input polarization states can be coupled into the TE-polarized modes of a pair of silicon waveguides, allowing high-efficiency coupling for all polarization states of the input fibre mode and realizing a *polarization-diversity coupler*. The superposition of two 1D-gratings evolves into a fibre coupler design based on photonic crystal array (PCA) of cylinders partially etched into the SOI platform [11–16] as shown in Fig. 1. In general, a fraction of the input fibre mode is coupled into both SOI waveguide arms of the structure, with the coupling efficiency into a given arm dependent on the polarization state of the fibre mode. The crucial figures of merit for a polarization diversity 2D-grating coupler are the total coupling efficiency (i.e. the sum of coupling efficiencies into the two Si waveguide arms), its bandwidth, and its sensitivity on the polarization of the input fibre mode.

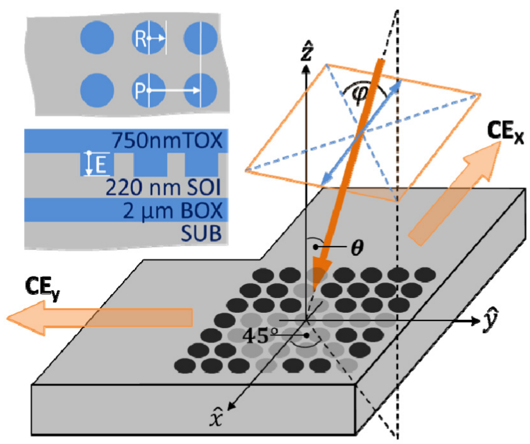

Fig. 1. Schematic of an input fibre mode in near-normal incidence to a 2D-grating coupler. The polarization state of the fibre mode is described by the angle of φ. The inset shows a schematic of the material cross-section, consisting of a 750nm top-oxide layer (TOX), a 220nm silicon-on-oxide (SOI) layer, a 2.0µm bottom-oxide layer (BOX), and semi-infinite substrate (SUB). The radius (*R*), pitch (*P*), and etch (*E*) parameters of the photonic crystal array are also indicated.

Because they are finite 3D systems, 2D-grating couplers can only be approximately described by the simple 2D-FDTD calculations used to optimize high performance 1D-grating couplers. However, in spite of this, 2D-grating couplers have been designed by extending and generalizing the results of 2D-FDTD calculations, followed by lithographic tuning, or by scaling-up the results of small-scale 3D-FDTD calculations on much reduced-scale test-structures [11–13]. Because of these limitations, it has not yet been possible to determine what the maximum theoretical coupling efficiency of a 2D-grating coupler may actually be, or to rigorously identify what combination of PCA parameters give rise to maximum or optimum coupling efficiency. Despite current design limitations, a number of 2D-grating coupler designs have been fabricated in the SOI platform that offer measured coupling efficiencies ranging from 20% (–7dB) [11,14] to 37% (–4.3dB) [15,16].

#189603 - $15.00 USD Received 29 Apr 2013; revised 3 Jun 2013; accepted 15 Jul 2013; published 6 Sep 2013

In this article, we report the first use of full 3D-FDTD calculations to systematically design and optimize the full 2D-grating coupler and waveguide region in a partially-etched SOI platform. A campaign of 3D-FDTD calculations is used to generate 72 different 2D-grating coupler designs that are each individually tuned to a peak coupling at 1550nm. Each one of these unique designs uses a different combination of etch-depth, hole-radius, and grating-pitch in the PCA that makes up the active region of the coupler. The simulation campaign essentially tests all possible combinations of PCA parameters that give coupling centred at 1550nm, and so allows us to rigorously identify the optimum 2D-grating coupler. The optimum combination of etch-depth, hole-radius, and grating-pitch offers the highest reported SOI 2D-grating coupler efficiency to date, along with a low sensitivity to the input polarization state of the fibre mode. This makes the optimized coupler design an ideal candidate for practical CMOS-compatible ICT applications. Additional 3D-FDTD calculations describe the propagation direction, mode-profile, and the polarization of the coupled mode. These data are important factors in the proper design of tapers and waveguides for integrated Si-photonic circuits, and are only provided by these full 3D-FDTD calculations – they cannot be extrapolated from existing approximations and simulations used previously for 2D-grating coupler design.

Calculations of photonic mode dispersion in the PCA by means of Guided Mode Expansion (GME) [17] provide an insight into the physical origin of the high efficiency coupling, and indicate that an optically active resonant guided mode in the PCA is responsible for the coupling. Since the results of the computationally lightweight GME calculations are shown to correspond closely to those of the far more computationally intensive 3D-FDTD calculations, a combined approach, using GME to generate good initial parameter estimates that are then fine-tuned by the 3D-FDTD calculations, may open the way for an efficient scheme for further optimization of the 2D grating coupler.

2. Description of simulation

A schematic of a 2D-grating structure is shown in Fig. 1. The 10.4μm MFD fibre mode is near-normally incident on the 11μm × 11μm PCA of the coupler with a $\theta = 15°$ angle-of-incidence in the plane that bisects the array at 45° (in order to create a symmetric condition between the two arms of the coupler). This non-normal angle of incidence supresses back-reflections into the fibre. The normalized intensities of light coupled into the arms aligned along the $\boldsymbol{x}$- and $\boldsymbol{y}$-axes are defined as the coupling efficiencies, CE_x and CE_y, respectively. The total coupling efficiency is then defined as $CE_T = CE_x + CE_y$. The most general description of the polarization state of a telecom fibre mode is elliptical, defined by the geometric angle of φ (which rotates in the plane spanned by the orthogonal vectors axes of $-\boldsymbol{x} + \boldsymbol{y}$ and, $\boldsymbol{x} - \boldsymbol{y} + \boldsymbol{z}\,\sin 15°$, see Fig. 1) and a phase term between these two axes projections. Since CE_x and CE_y are defined in terms of intensities and not fields (i.e., $I = |E|^2$), the coupling efficiency into a given arm depends only on the geometrical polarization angle of φ.

The commercial package *FDTD Solution*™ from *Lumerical Inc*. is used to make fully 3D-FDTD simulations of the 15μm × 15μm × 5μm volume surrounding the 2D-grating coupler. As shown in the inset of Fig. 1, the PCA is defined in an industrially standard SOI wafer, with a 220nm Si layer on a 2.0μm bottom-oxide layer (BOX) grown on a Si substrate. To support the process flow for other integrated components to be added to the Si-photonic circuit, a 750nm top-oxide layer (TOX) is included in the simulation. The SiO_2 of the TOX is assumed to fully and perfectly fill the holes of the PCA. The refractive index of the SOI slab and the Si substrate at 1550nm is taken as $n_{Si} = 3.47$, and the refractive index of the TOX and BOX as $n_{OX} = 1.44$.

An integrated conformal mesh algorithm is used to optimize the mesh of the simulation volume, prioritizing the high spatial resolution for regions in which variations in refractive index are strongest, i.e. the PCA and the interfaces between the SOI wafer layers. Our medium mesh calculations have a spatial resolution of 20nm ≈1550nm/(20 × n_{Si}) in the region of the PCA and approximately half that resolution in the BOX and TOX layers. Convergence tests of the mesh dimensions confirmed that this resolution is sufficient to accurately describe the physics of the 2D-grating coupler. A single medium mesh simulation of the 15µm × 15µm × 5µm coupler volume takes ≈90 minutes on a 3.6GHz QuadCore Desktop PC. (Note - approximately 250 simulations were needed to generate the contour plot in Section 3. Therefore, identifying the parameters for peak coupling efficiency took approximately two weeks of pure computation time. Only recently has it become practical to perform such a computationally intensive campaign for device optimization, even using commercial software). The light intensity coupled into the 10µm × 220nm SOI strip waveguides of the coupler is measured using power-field monitors placed ≈4µm from the edge of the PCA. Even in the near-field of the coupler, these monitors return a transmission spectrum that is equal to within ± 1% of that measured in the far-field, i.e. ≈70µm from the centre of the PCA.

The telecom fibre mode is simulated by a Gaussian source centred at 1550nm, with a 10.4µm MFD. In our simulation, the fibre mode is incident on the coupler, and the 3D-FDTD calculations fully account for the angle of incidence and the 2D intensity profile of the fibre mode. The tilted fibre-end is assumed to just touch the surface of the TOX layer. Given the 125µm diameter of the outer core, this means that the input mode exits the fibre ≈16µm above the TOX and slightly diverges (numerical aperture = 0.14) before it is incident on the PCA. The 3D-FDTD calculations allow this 16µm stand-off distance to be directly included in the mathematical definition of the Gaussian source, and so it is not necessary to incorporate the stand-off into the simulation volume. Within the Rayleigh length of the fibre (≈50µm), a variation in the stand-off distance has only a slight impact on coupler performance that can be first-order corrected by using a slightly larger PCA area. The coupling efficiency depends of the lateral fibre position, and does not necessarily correspond to the fibre being centred on the PCA. The optimum fibre position for a given coupler design is determined by displacing the fibre mode across the photonic crystal array, along the 45° line shown in Fig. 1, until the condition of maximum coupling is found. This fibre mode alignment can be done using low mesh simulations.

To date, there have been no reports of other computational approaches to simulating the coupling efficiencies of 2D-grating couplers, and so a direct cross-check of our methodology is not possible. However, our 3D-FDTD calculations have successfully reproduced the results of existing 2D-FDTD calculations of 1D-grating couplers [4], and also the experimentally measured coupling spectra of 2D-grating couplers [11] with a good degree of accuracy. Using 3D-FDTD calculations to simulate the coupling efficiency of 1D-grating couplers is advantageous to the current approach of using of 2D-FDTD, because it removes the need to apply a mathematical overlap function (used to approximate the modal acceptance of the fibre) to the results of 2D-FDTD calculations [4], before being able to extract the coupling efficiency. For the 2D-grating coupler fabricated and characterized in [11], the measured coupling efficiency is 20% (−7.0dB), the central wavelength is 1505nm, and full-width half maximum line-width is 60nm. Our 3D-FDTD calculations agree very well with these measured values; we calculate a coupling efficiency of 21.5% (−6.7dB), a central wavelength of 1488nm, and a line-width of 70nm.

3. Optimizing coupling efficiency

The coupling efficiency of a 2D-grating coupler is largely determined by the properties of its PCA. As illustrated in Fig. 2, both the peak efficiency and central wavelength of coupling depend sensitively on the etch-depth (*E*), hole-radius (*R*), and grating-pitch (*P*) of the PCA. Note that CE_y with $\varphi = 45°$ is chosen as the default means of expressing the coupling efficiency, because it corresponds closely to the mean CE_T of the 2D-grating coupler averaged over all possible input polarization states, as will be shown later in Section 4. For the 2D-grating coupler described in Section 2, with fixed hole-radius of 215nm and a grating-pitch of

616nm, the variation in coupling as a function of etch-depth can be seen in Fig. 2(a). Deeper etching of the PCA results in a blue-shift of the coupling, and the highest coupling efficiency is achieved with an etch-depth of ≈110nm, but is not centred on the target wavelength of 1550nm.

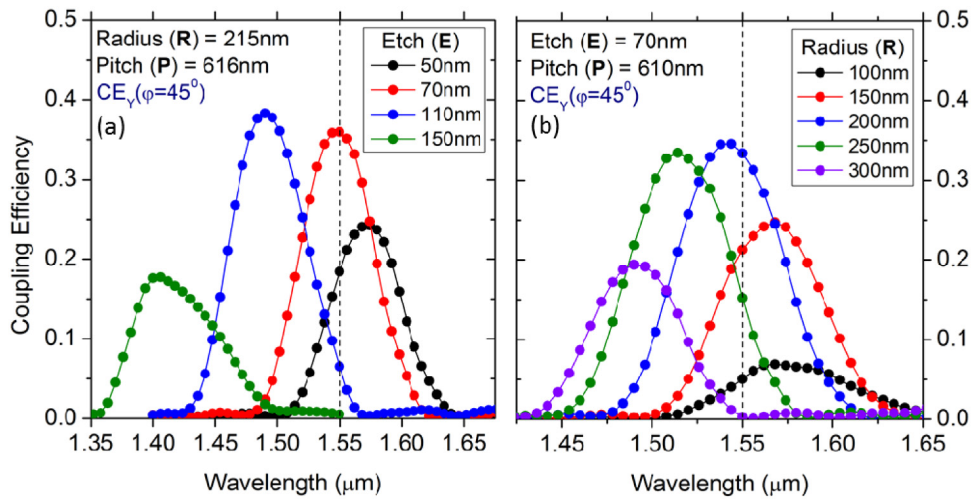

Fig. 2. (a) The coupling spectra of a 2D-grating coupler with fixed radius (*R*) and pitch (*P*) and a series of different etch-depths (*E*). CE_y(φ = 45°) is used to express the coupling efficiency, because it closely matches the average performance of the coupler over all possible input polarization states. (b) The coupling spectra of a 2D-grating coupler with fixed etch-depth and pitch and a series of different hole radii.

A similar trend is observed in Fig. 2(b), where the 2D-grating coupler is simulated with a constant etch-depth of 70nm and grating-pitch of 610nm, but a variable hole-radius. As the hole-radius is increased, the coupling spectra blue-shift, and the highest coupling efficiency appears to be with *R*≈225nm, but at a wavelength of ≈1525nm, which is again offset from the 1550nm target.

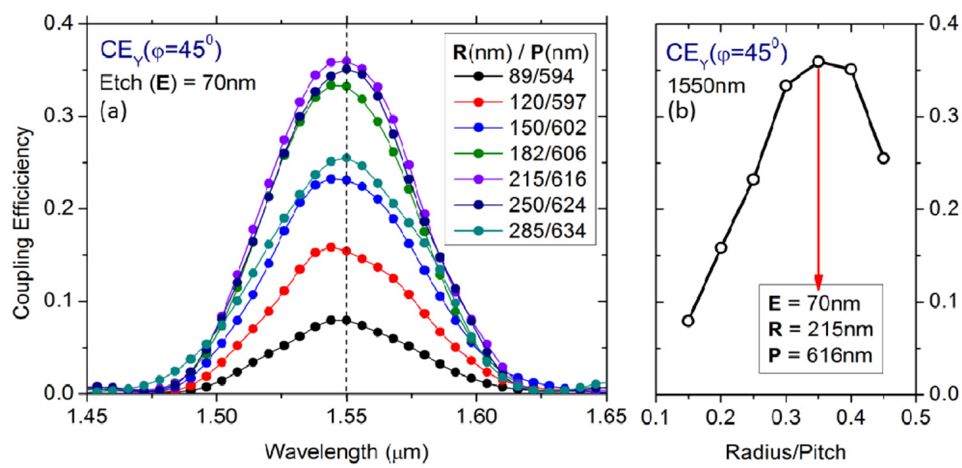

Fig. 3. (a) A series of hole-radius (*R*) and grating-pitch (*P*) pairs for a partial etch-depth (*E*) of 70nm that tune the coupling to 1550nm (b) Identifying the radius-pitch pair that gives highest coupling efficiency value for the 70nm etch design.

In order to tune the 2D-grating coupler to 1550nm, it is necessary to simultaneously adjust the hole-radius and grating-pitch of the PCA. The coupling spectra of a selection of these 3D-

FDTD "tuned" radius and pitch pairs, providing coupling centred at 1550nm for a 70nm etch-depth, are shown in Fig. 3(a). While each of these radius-pitch pairs gives their maximum coupling at 1550nm, they each do so with different coupling efficiencies. As shown in Fig. 3(b), when the coupling efficiency at 1550nm is plotted as a function of the ratio between the radius and pitch of these pairs, it is easy to identify the optimum combination. For a 2D-grating coupler with an etch-depth of 70nm in a 220nm SOI slab, the best choice would be a hole-radius of 215nm, and grating-pitch of 616nm, which gives a coupling efficiency of 37% (−4.3dB) at 1550nm.

When analogues of Fig. 3(b) are generated for a series of different etch-depth that span the 220nm SOI slab thickness, a contour plot can be built up that quantifies the peak coupling efficiency at 1550nm for the full span of possible etch-depths, hole-radii, and grating-pitches. The contour plot of Fig. 4 is made up of the peak coupling efficiency values from 72 unique 2D-grating coupler designs, all of which have been individually tuned to 1550nm [as in Fig. 3(b)]. The peak in this contour plot corresponds to the highest possible coupling efficiency that can be achieved within the boundary conditions of the simulation, i.e. with a uniform 2D-grating coupler design etched in a 220nm SOI slab with 750nm TOX and 2.0μm BOX.

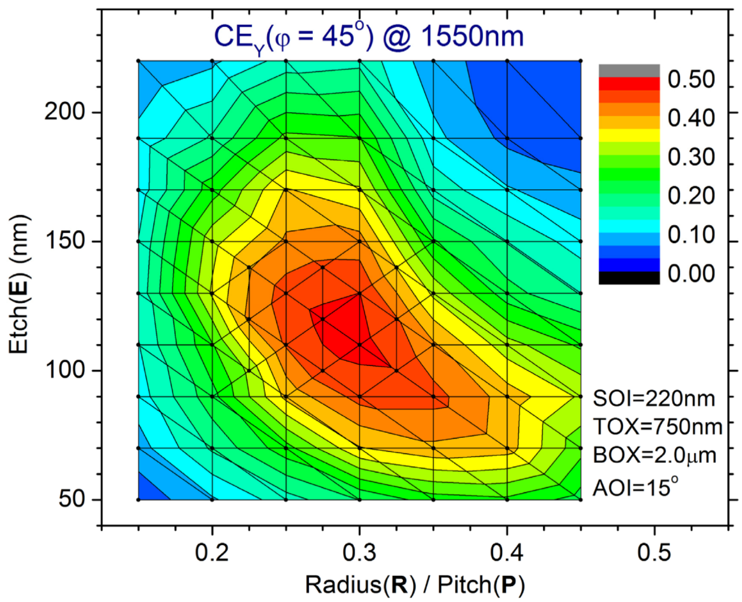

Fig. 4. The contour plot of coupling efficiency at 1550nm for a 2D-grating coupler realized in 220nm SOI, with the given BOX and TOX thicknesses, as a function of etch-depth and the ratio of hole-radius and hole-pitch. The peak coupling efficiency in this contour map corresponds to the globally optimized coupler parameters for the system.

The optimum PCA parameters are E = 120nm, R = 185nm, and P = 635nm, and the 2D-grating coupler based on these parameters gives $CE_y(\varphi = 45°) = 48\% = -3.2$dB. This coupling efficiency is more than double that reported from measurements of existing uniform SOI 2D-grating couplers [11,14]. Furthermore, the coupling efficiency of our 3D-FDTD optimized design exceeds that reported from the best non-uniform curved SOI 2D-grating couplers into single-mode SOI waveguides, (which benefit from a natural grating apodization) by ≈1dB [16]. In fact, the 3D-FDTD optimized design just exceeds the highest reported measurement of coupling efficiency from a 2D-grating coupler, which is 47% (−3.3dB) from a non-CMOS compatible design using a flipped benzocyclobutene (BCB) bonded InP membrane with integrated vapour deposited gold mirror [12]. Our results indicate that, in order to improve coupling performance, it is necessary to etch deeper than the standard 70nm partial etch depth in the 220nm SOI wafer that is used in many existing contemporary designs [14–16].

The typical sensitivity of the coupling efficiency to fabrication tolerances in the etch-depth, and hole-radius can be seen directly in Fig. 3(a) and (b). For the specific case of the optimum PCA parameters identified in Fig. 4, a variation of + 10nm/-10nm in the etch-depth translates to a change in the mean coupling efficiency of + 1%/-2% and a shift in wavelength of −12nm/+10nm. Similarly, a variation of + 10nm/-10nm in the hole-radius translates to a change in coupling efficiency of −3%/+1%, and a wavelength shift of + 10nm/-10nm. Finally, a variation of + 10nm/-10nm in the grating-pitch translates to a change in the mean coupling efficiency of −3%/+0.5% and a shift in wavelength of + 20nm/-19nm.

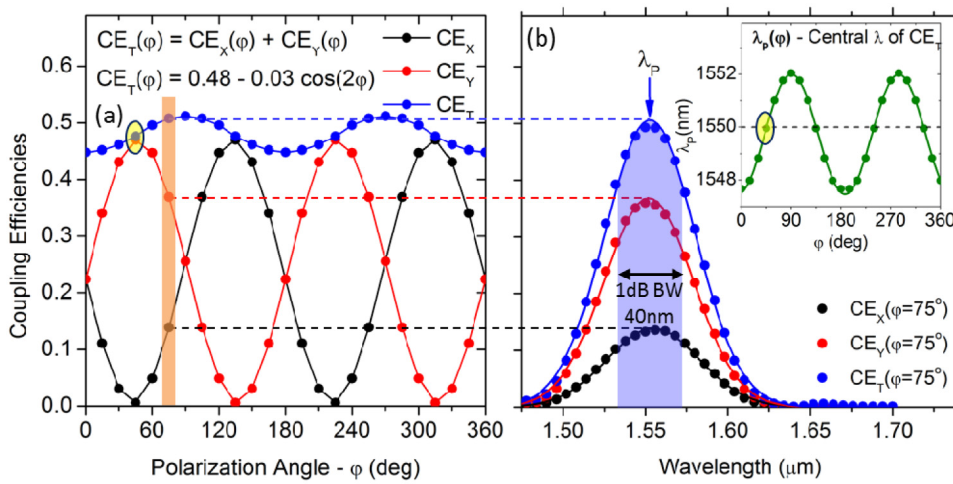

Fig. 5. (a) The variation of CE_x, CE_y, and CE_T as a function of the input polarization angle of φ for the 2D-grating coupler based on the optimum PCA parameters. The trigonometric fit to determine the mean value of CE_T and its variation with φ is also given. Note that CE_y(φ = 45°) closely matches the mean value of CE_T. (b) The coupling spectra of CE_x, CE_y, and CE_T for φ = 75°, fitted with Gaussian line-shapes. The inset shows the small but systematic variation of the central wavelength of CE_T as a function of φ. Again, the central wavelength of CEy(φ = 45°) closely matches that of the mean CE_T.

4. Sensitivity to input polarization

Ideally, the total coupling efficiency (i.e. $CE_T = CE_x + CE_y$) of a 2D-grating coupler is completely insensitive to the polarization state of the input fibre mode. However, the fibre tilt used to provide directionality and reduce back-reflections, breaks the ideal symmetry, and introduces a polarization sensitivity that has been experimentally observed [12,13]. In Fig. 5(a), 3D-FDTD calculations are used to model the variation of the CE_x, CE_y and CE_T as a function of the input polarization, for the 2D-grating coupler based on the optimum PCA parameters (i.e. E = 120nm, R = 185nm, and P = 635nm). As the input polarization is swept through 360°, CE_x and CE_y vary from 0.6% to 47%, giving an extinction ratio of −19dB. However, CE_T(φ) is far less dependent on the input polarization, varying only between 45% (−3.5dB) and 51% (−2.9dB) during the sweep. This shows that, in addition to generating a 2D-grating coupler with a high mean coupling efficiency, the optimum PCA parameters also offer a low sensitivity to the polarization state of the fibre mode. From Fig. 5(a) it is clear that CE_y(φ = 45°) closely corresponds to the mean value of CE_T(φ) averaged over all values of φ, and so (as mentioned in Section 3) is a good choice as a representative coupling efficiencies for optimization and illustration

In the general case, the fibre mode is unevenly coupled into the two SOI waveguides of the 2D-grating coupler. Figure 5(b) illustrates the case of φ = 75°, where CE_x/CE_y ≈0.37. The

#189603 - $15.00 USD Received 29 Apr 2013; revised 3 Jun 2013; accepted 15 Jul 2013; published 6 Sep 2013

line-shape of the CE_T, CE_x, and CE_y spectra are all Gaussian, with a 1dB bandwidth of 40nm for CE_T. In analogy to the slight variation in the magnitude of CE_T as a function of φ, the central wavelength of CE_T also varies slightly around a mean value of 1550nm during the φ sweep. The magnitude of this oscillation (1548nm < λ_P < 1552nm) is one order of magnitude less than the 40nm 1dB bandwidth, and so does not represent a significant performance limitation. Again, the central wavelength of CE_y(φ = 45°) closely corresponds to the mean central wavelength averaged over all values of φ, confirming CE_y(φ = 45°) as a good choice for the representative coupling efficiency for optimization.

5. Mode propagation, profile, and polarization

Additional 3D-FDTD calculations are used to generate spatial mapping of the light coupled from the fibre mode into the SOI slab, to investigate its propagation direction, mode-profile and polarization dependence. These calculations need comparatively large simulation volumes, typically 70μm × 20μm x 5μm, and take >10 hours with the medium mesh resolution.

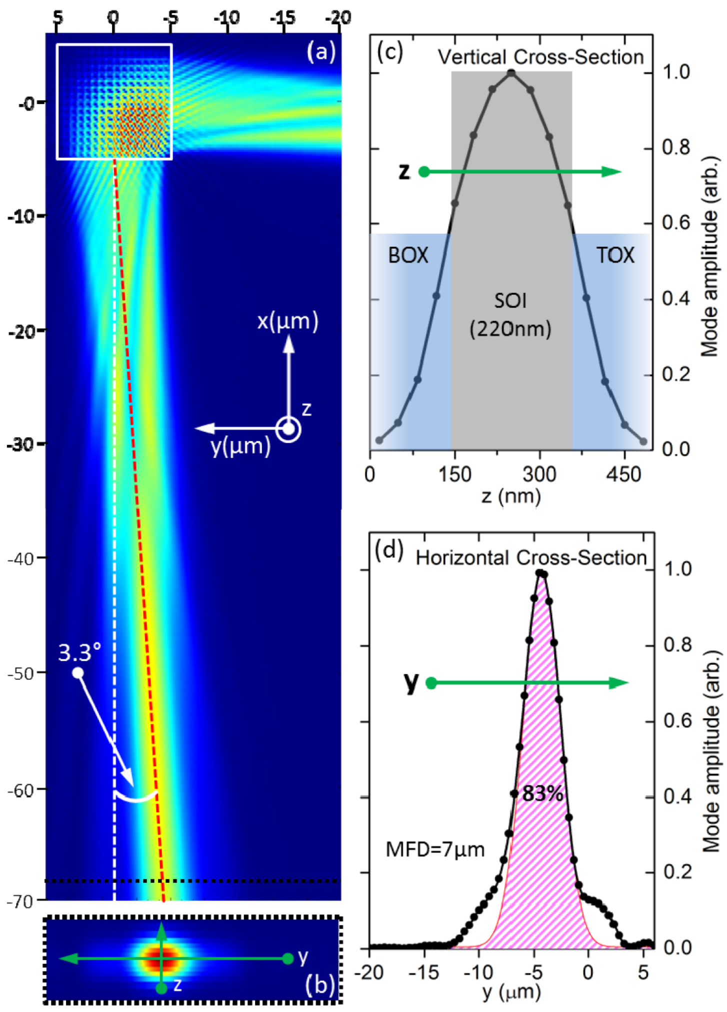

Fig. 6. (a) The propagation map of light coupled from the fibre mode into a SOI layer from a photonic crystal array based on the optimum PCA parameters. (b) A contour plot of the coupled mode at a distance of 68μm from the edge of the PCA. (c) and (d) The vertical and horizontal cross-sections of the contour plot in (b).

Figure 6(a) shows the propagation of light from the 11µm × 11µm PCA based on the optimum parameters into the SOI slab. To observe the natural and undisturbed propagation of the coupled mode, it is necessary to remove the SOI waveguides and replace them with the full SOI slab. In these simulations, the input fibre mode is aligned centred on the PCA, and φ is set to 0° in order to give a symmetric coupling condition in both ***x*** and ***y*** directions. The coupled mode does not propagate precisely along the ***x***- and ***y***-axes of the PCA, but at a small angle of 3.3° to these axes. This result is in agreement with experimental observations of similar angular offsets effects in 2D-grating coupler systems, where empirical lithographic tuning of the waveguide structures have indicated an angular offset of 2.8° in analogous couplers [12,13]. This angular offset arises from the slight tilting of the input fibre mode with respect to the coupler.

After ≈50µm of propagation, the coupled mode recovers a single-mode-like profile. The intensity profile of the coupled mode at a distance of 68µm from the edge of the PCA is shown in Fig. 6(b), with horizontal and vertical cross-sections in Figs. 6(c) and (d). In the vertical direction (i.e. along the ***z***-axis), the mode is symmetrically confined in the 220nm SOI slab, but with significant overlap into the BOX and TOX layers. In the horizontal direction (i.e. along the ***y***-axis), 83% of the mode is bounded by a Gaussian peak with $1/e^2$-width of 7µm, which is somewhat narrower than the 10.4µm MFD of the input fibre mode. The remaining 17% of the light is distributed broadly over a 15µm cross-section in broad lobes. This propagation mapping and mode profile determination cannot be generated by the simplified 2D-FDTD calculations used for earlier 2D-grating coupler design approximations, and so the 3D-FDTD calculations provide important new information for the designs of optimized integrated tapers that channel light from the 2D-grating coupler into the single-mode SOI waveguides for distribution to the rest of the photonic circuit.

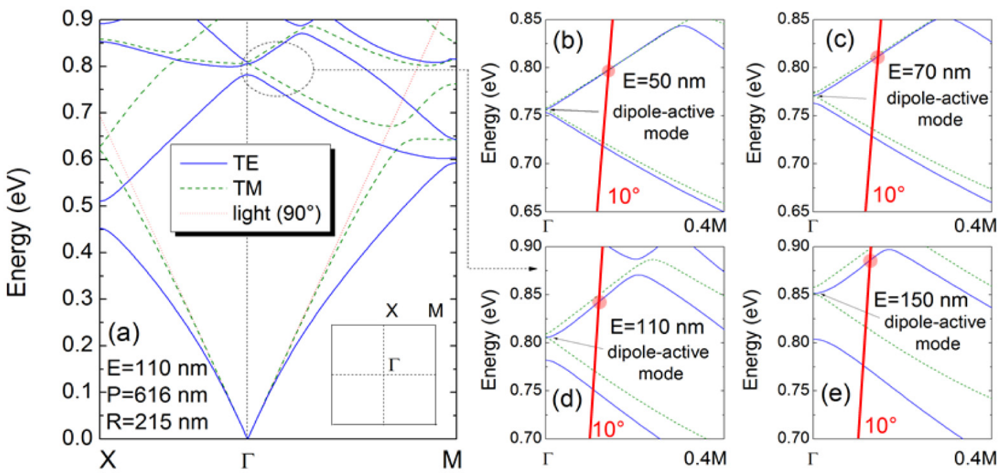

Fig. 7. (a) Energy band dispersion for the 2D grating coupler with 110 nm etch depth, 215 nm hole radius, and 616 nm lattice constant, as calculated by multi-layer guided-mode expansion. The main symmetry directions in the Brillouin zone of the square lattice are indicated. Modes are classified as even (TM, dashed lines) or odd (TE, full lines) with respect to the vertical plane of incidence, which changes with the symmetry line (see text). The light line corresponding to 90° incidence from the TOX layer is also plotted. (b-e) Close-up of the photonic mode dispersion along the Γ−M direction and close to the normal incidence for different etching depth of the holes in the SOI layer, as indicated in each panel. The 10° light line is also shown, and the crossing point with the TE-like dipole-active mode corresponding to the peak in coupling efficiency is highlighted.

Optoelectronic devices for integrated photonic circuits, such as Mach-Zender modulators and semiconductor optical amplifiers are typically optimised for TE-polarization. As such, any TM-polarized component of the coupled mode is a practical loss to the circuit. We define the polarization extinction ratio (PER) as the ratio between the TE-polarized intensity and TM-polarized intensity of the coupled mode. The PER can be determined from the same power field monitors used to determine the mode profiles in Fig. 6. When the mode is coupled equally into both arms (i.e. φ = 0°, 90°, 180°, etc.), then the PER is −24dB, and when it is preferentially coupled into a single arm (i.e. φ = 45°, 135°, 225°, etc.) then the PER is −25dB. This shows that the optimum PCA parameters give a 2D-grating design with a very low proportion of TM-polarized light in the coupled mode.

6. Origin of coupling

3D-FDTD calculations can be used to generate the optimum PCA parameters for a given 2D-grating coupler design, but they do not provide much insight into the coupling mechanism. Guided mode expansion (GME) calculations [17] can give a more comprehensive picture of the physics in play by describing the photonic mode dispersion of the PCA. GME is based on solving the 2nd-order Maxwell equation, after expanding the electromagnetic field in terms of a separable basis of plane waves in the plane, and guided modes of the vertical dielectric stack. Within this formalism, the photonic modes of the PCA are radiatively coupled to propagating modes in the TOX and BOX by perturbation theory. The main assumptions of GME are that (i) guided modes are coupled to radiative modes of an effective waveguide with a refractive index averaged over a unit cell of the PCA, and (ii) 2nd-order corrections to the resonance energies of the guided modes (induced by coupling to the radiative modes) are not taken into account [17].

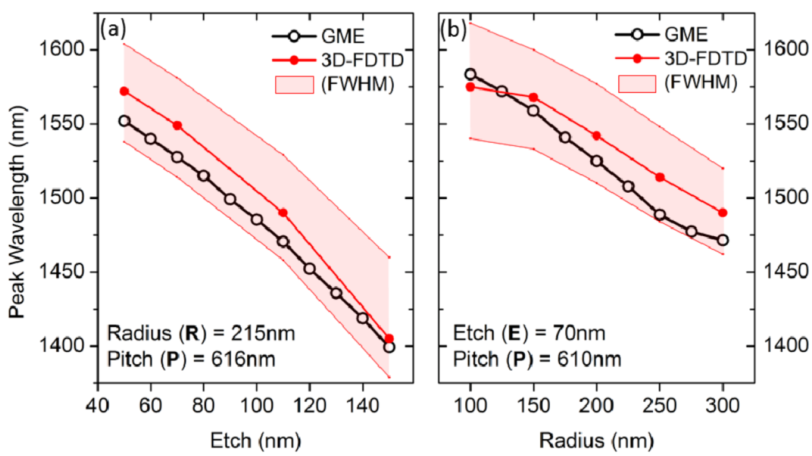

Fig. 8. (a) A comparison of the resonant wavelength from the crossing of the 10° light line and the GME calculated dipole-active TE mode along the Γ-M direction, and the peak coupling from 3D-FDTD calculations, as a function of etch-depth. (b) The same comparison as for (a) with fixed etch-depth and pitch, but variable hole radius. The shaded areas correspond to the full-width half-maximum (FWHM) of the 3D-FDTD peaks (see Figs. 2 and 3).

Figures 7(a-e) shows a series of GME-calculated photonic band dispersion diagrams for the PCAs with the same parameters (radius, pitch, and etch) as those shown in the 3D-FDTD calculations of Fig. 2(a). The dipole-active mode is doubly degenerate at the Γ point ($\boldsymbol{k}$ = 0) in the first Brillouin zone of the square lattice, and increased etch-depth leads to a greater splitting of the photonic bands. The energy of the coupling resonance is given by the crossing of the 10° light line of the input mode with the TE-like dipole-active modes of the PCA. The 10° light line in the GME corresponds to the 15° angle of incidence used in the 3D-FDTD calculations, after refraction by the TOX layer.

As shown in Figs. 8(a) and (b), the coupling resonance predicted by GME is in excellent agreement with the peak of the 3D-FDTD calculated coupling spectra of Figs. 2(a) and (b).

This agreement is better than 25nm and always within the full-width half-maximum of the spectra line-width. This strong correspondence between the two numerical approaches is an important result. GME calculations require negligible computational effort, but assume an infinitely extended PCA with semi-infinite BOX and TOX layers, while, in contrast, 3D-FDTD is computationally intensive, but more fully accounts for the finite dimensions of the simulated structure and waveguide coupling. The correspondence shown in Figs. 8(a) and (b) indicates that the fast GME calculations can be used to generate reliable initial values for the 2D-grating design that then need only be fine-tuned by 3D-FDTD calculations to account for the finite dimensions of the coupler structure. This opens the way for a more global optimization of the 2D-grating coupler over a wide parameter-space that includes not only the hole-radius, grating-pitch, and etch-depth, but also SOI layer thickness, angle-of-incidence, etc. This level of optimization is not currently practical with desktop 3D-FDTD calculations alone, because they are too computationally intensive. The combination of joint GME and 3D-FDTD optimization may lead to significantly improved coupling performance by determining the absolute best combination of many different design parameters.

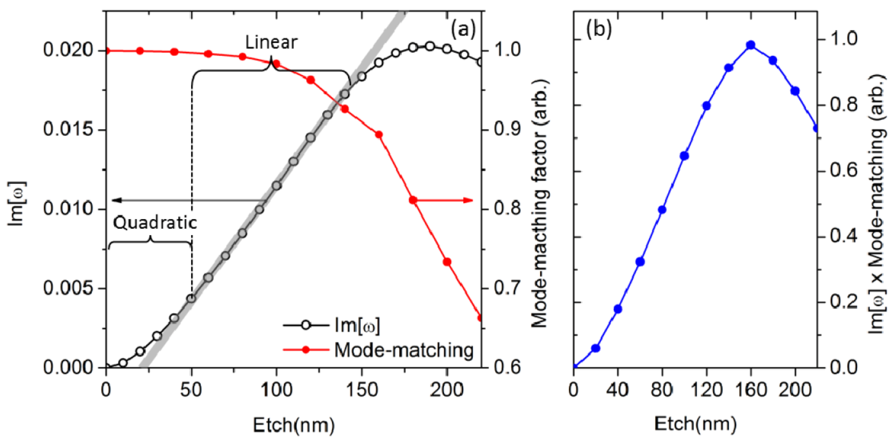

Fig. 9. (a) The imaginary part of the wave-vector (proportional to coupling strength) from the GME calculations in Fig. 7(a), and an estimate of the mode-matching between the photonic crystal and the SOI waveguide, as a function of etch-depth. (b) The product of the two terms from (a) showing that the maximum effective coupling between the fibre mode and the SOI waveguide is expected for an intermediate etch-depth of the order of half the SOI layer thickness

In addition to predicting the resonance energy of a given PCA, the GME calculations also generate the imaginary part of the frequency, Im[ω], which is qualitatively proportional to the coupling strength of the PCA [18]. As shown in Fig. 9(a), for the PCA described in Figs. 2(a) and 8(a), increasing the etch-depth increases Im[ω] and so also the coupling strength. For shallow etch-depths, the increase is quadratic, in line with perturbative coupled mode theory for waveguide gratings, but for etch-depth >40nm the increase is linear, which indicates that the PCA has entered the regime of a strongly modulated photonic crystal slab. While deeper etching leads to greater coupling strength in the PCA, it also leads to poorer mode-matching between the PCA and the SOI waveguides of the 2D-grating coupler, because of differences in effective index and vertical mode displacement. A qualitative measure of the variation of this mode-matching as a function of etch-depth can be estimated from back-reflection calculations (using a mode-source launched from the SOI waveguide side towards the PCA) made using 3D-FDTD simulations, and is also included in Fig. 9(a). The product of the coupling strength from Im[ω] and the mode matching factor is shown in Fig. 9(b), and should be qualitatively proportional to the coupling efficiency of the corresponding 2D-grating couplers. Indeed, the results of this very approach generate the same qualitative trend as that

#189603 - $15.00 USD Received 29 Apr 2013; revised 3 Jun 2013; accepted 15 Jul 2013; published 6 Sep 2013

observed in full 3D-FDTD determinations, see Fig. 4 – the highest 2D-grating coupler efficiency with a given hole-radius and grating-pitch tends to be achieved with an intermediate etch-depth that is of the order of half the SOI slab thickness.

Conclusion

We have presented a systematic campaign of 3D-FDTD calculations leading to the optimum parameters of a photonic-crystal based 2D grating coupler to provide the highest coupling efficiency from a single-mode fibre into Silicon-on-Insulator waveguides at 1550 nm. The optimum parameters for the etch depth and for the photonic crystal array give a high mean coupling efficiency of 48% (−3.2dB). An analysis of polarization dependence shows that the coupling efficiency is only weakly sensitive to the polarization state of the input fibre mode. 3D-FDTD propagation mapping of the coupled mode provides important information for the designs of optimized integrated tapers for coupling into narrow, single-mode waveguides. Calculations of photonic mode dispersion by means of guided-mode expansion indicate that the coupling mechanism originates from an optically active resonant guided-mode in the photonic crystal array. The results of the computationally lighter mode-expansion calculation correspond closely to those of the more intensive 3D-FDTD simulations, and they allow interpreting the optimal etch depth as resulting from simultaneous optimization of coupling from the fibre into the grating, and from the grating into the silicon waveguides. Using guided mode expansion to generate good initial values for optimized 2D-grating designs, which then need only to be fine-tuned using 3D-FDTD calculations, opens the way for a global optimization over a larger parameter space, which may lead to further improved performance of the 2D grating coupler.

Acknowledgments

This work was supported by the EU through FP7-ICT-2011-8 Contract No. 318704 "FABULOUS."